Generation mechanism of NO_x and N_2O precursors (NH_3 and HCN) from aspartic acid pyrolysis: A DFT study

Kang Peng[1], Qin Wu[2*], Fu Zongqiang[3], Wang Tipeng[2], Ju Liwei[1], Tan Zhongfu[1]

(1. *Institute of Energy Economics and Environment, School of Economics and Management, North China Electric Power University, Beijing 102206, China*; 2. *National Engineering Laboratory for Biomass Power Generation Equipment, School of Renewable Energy Engineering, North China Electric Power University, Beijing 102206, China*; 3. *School of Materials Science and Mechanical Engineering, Beijing Technology and Business University, Beijing 100048, China*)

Abstract: In order to better understand the mechanism of NO_x and N_2O precursors (NH_3 and HCN) from aspartic acid (Asp) pyrolysis, decomposition reaction networks resulting in the generation of NH_3 and HCN were investigated by employing density function theory methods. After several pathways were analyzed in detail, two series of pyrolytic reactions containing three possible pathways were proposed. All the reactants, transition states, intermediates and products were optimized, also the electronic properties on these crucial points were discussed, which shows that C_α acts as the most active site to initiate the pyrolysis reaction, where the direct C_α-C_β bond breakage, due to the atomic charge population of repulsion, led to one key route for the generation of HCN, and the transfer of H_α from C_α to C_β resulting in another key route for the generation of HCN, while the transfer of H_α from C_α to N atom of Asp resulting in the key route for the generation of HN_3. Further, the kinetic analysis based on speed control method in each key reaction pathway was conducted to further compare the generation of HCN and NH_3 under various temperatures. The above results are in accordance with the related experimental results.

Keywords: pyrolysis, aspartic acid (Asp), amino acid, DFT

DOI: 10.3965/j.ijabe.20160905.2559

Citation: Kang P, Qin W, Fu Z Q, Wang T P, Ju L W, Tan Z F. Generation mechanism of NO_x and N_2O precursors (NH_3 and HCN) from aspartic acid pyrolysis: A DFT study. Int J Agric & Biol Eng, 2016; 9(5): 166－176.

1 Introduction

Biomass has the largest utilization scale of renewable energy and ranks fourth in the total energy consumption which is just next to coal, oil, and natural gas[1]. Thermal utilization of biomass mainly includes pyrolysis, gasification and combustion. During biomass pyrolysis and gasification, the fuel-N will be converted to volatile-N (NH_3, HCN, NO and HNCO), as well as char-N and tar-N[2-9]. Ammonium salt crystallizations can be formed by the reaction of NH_3, CO_2 and H_2O, which affect the security and long-term stable operation of the systems. HCN is a highly toxic gas which should be removed by complex purification device[10-12]. In the process of biomass combustion, volatile-N, tar-N and char-N will be oxidized to NO_x, N_2O and other nitrogen oxides, resulting in acid rain and photochemical smog which destroy the atmosphere and affect human health[13].

It has been demonstrated that the main nitrogen functionalities in biomass exists in proteins and amino acids together with some other forms such as DNA, RNA, alkaloids, porphyrin and chlorophyll[10,11]. Pyrolysis is the primary step of biomass gasification and combustion. Therefore, many efforts have been conducted to study the N-containing species in the gas products and tar. NH_3

Received date: 2016-04-28 **Accepted date:** 2016-07-17

Biographies: Kang Peng, PhD, research focus on lignocellulose mechanism and economics research, Email: kangpeng19821125@163.com; **Fu Zongqiang**, Associate Professor, research focus on material science, Email: fuzongqiang@btbu.edu.cn; **Wang Tipeng**, Associate Professor, research focus on lignocellulose utilization, Email: wtp_771210@163.com; **Ju Liwei**, PhD, research focus on bio-energy economics, Email: 183758841@qq.com; **Tan Zhongfu**, Professor, research focus on energy economics, Email: tanzhongfubeijing@126.com .

***Corresponding author: Qin Wu**, Associate Professor, research focus on lignocellulose mechanism simulation. Mailing address: National Engineering Laboratory for Biomass Power Generation Equipment, School of Renewable Energy Engineering, North China Electric Power University, Beijing 102206, China. Tel: +86-10-61772457, Email: qinwugx@126.com.

and HCN are the main forms of volatile-N and the yields of NO and HNCO are relatively low. Michaël et al.[14] investigated that NH_3 is the main N-compound with increasing temperature until reaching a plateau at 825-900°C, while HCN release is increasing sharply with temperature which attribute to the volatile-N cracking and secondary reactions. Biomass size and heating rate have significant effects on the selectivity of N-conversion during pyrolysis as it will influence the thermal conditions and consequently the eventual secondary reactions in the sample[15,16]. Different types of biomass also have different nitrogen release characteristics, which are mainly determined by the occurrence of nitrogen in biomass. It is known that cellulose, hemicellulose and lignin are the major components in biomass and the correlation of these components on the N-containing release behavior have been conducted by several researchers. Lignin may promote formation of heterocyclic nitrogenous compounds which then decompose to form of HCN[17]. In presence of cellulose, hemicellulose and lignin, the content of char-N was significantly increased during amino model compound pyrolysis[18]. Biomass contains considerable amounts of alkaline earth metallic species (AAEMs) from the soil during growth. A significant effect on N-containing species release by AAEMs during biomass pyrolysis has been revealed by Ren et al.[19] Potassium salts can promote N-conversion to volatile-N at lower temperature for activation energy decreasing, but restrain the total yields of the N-containing species. With the addition of CaO, the total yields of HCN and NH_3 decrease in the whole pyrolysis temperature region.

As mentioned above, fuel-N conversion paths during biomass pyrolysis are affected by several conditions including heating rate, final temperature, biomass fuel type, reactor form and residence time, etc., which is difficult to obtain clear fate of fuel-N. Therefore, N-containing model compound such as yellow peas, soya beans, whey protein and different kinds of amino acids to selected to study the transformation of nitrogen[15,16,20,21]. The pyrolysis of model compounds would lead to increasing insight regarding the formation of N-containing species from biomass pyrolysis. These studies investigated that HCN, NH_3 and HNCO are the main pyrolysis products from proteins and amino acids which greatly affects the distribution of volatile-N and char-N as well as HCN/NH_3 selectivity[15,16]. It is identified that nitrogen bound in the proteins and amino acids is the main source of NH_3, and heterocyclic nitrogen is the main source of HCN during pyrolysis especially at the temperature higher than 800°C. It was proved that the yields of HCN, and NH_3 and nitrogen conversion pathway from amino acid pyrolysis are influenced in the presence of AAEMs. The primary decomposition of the amino acid as well as the secondary cracking pathway of 2, 5-piperazinedione are both catalyzed by AAEMs. Mineral matter also has catalytic effects on the thermal cracking of nitrogen-containing char for amino acids with reactive side chains[20,21].

Although extensive experimental studies on amino acid pyrolysis under different conditions have been carried out, few theoretical studies have systematically analyzed the detailed mechanism of amino acid decomposition for the generation NO_x and N_2O precursors (NH_3 and HCN). Experimental studies usually detected the pyrolysis characterization based on the analysis of the final products. However, the key reaction pathway leading to the generation of NH_3 and HCN involves various intermediates and the related electronic interactions between atoms, which remain unknown. To solve this issue, the present study selected aspartic acid (Asp) as the probe amino acid molecule and focuses on the mechanisms of NH_3 and HCN generation resulted by direct bond breakage and hydrogen transport in Asp, revealing the key pathways to the final generation of NH_3 and HCN during Asp pyrolysis. Following the key steps, electronic properties of the crucial points were detected to reveal the electronic interactions between atoms and the active site within the Asp molecule. Further, the kinetic models of the strategic routes under different temperature were described. Results can provide fundamental understanding of Asp pyrolysis for controlling the generation of NH_3 and HCN.

2 Computational details

The detailed equilibrium geometries and electronic

properties of the reactant, intermediates, transition states and products involved in every chemical reactions were performed using density functional theory (DFT) calculations, which were employed in the present study within the DMol^3 package. The exchange-correlation energy of electrons was calculated with the spin-polarized generalized gradient approximation (GGA)[22] as implemented in the DMol^3 package. The Perdew-Burke-Ernzerhof (PBE) exchange-correction functional[23] and the double numerical plus polarization (DNP)[24-26] basis set were used throughout the calculations, which is equivalent in accuracy to the commonly used 6-31G** of Gaussian orbital basis set. But the numerical basis set is much more accurate than a Gaussian basis set with the same size. During the calculations, atoms were relaxed and Brillouin zone integration was performed at the gamma point[27]. Calculations adopt an energy convergence tolerance of 1×10^{-6} Ha and gradient convergence of 1×10^{-6} Ha/Å. A formulation for the linear (LST) and quadratic synchronous transit (QST) methods was used to search the transition states[28,29], which had exactly one imaginary frequency while the reactant, intermediates and products had no imaginary frequencies. Standard thermodynamic changes are energy differences between the reactants and the products, including the ZPE. Energies of optimized reactants and products at different temperatures (673 K, 773 K, 873 K, 973 K and 1073 K) were calculated in frequency calculation route section in reference to the work of Zhang et al.[30]

The Asp molecule was modeled and the stable configuration was obtained after geometric optimization, as shown in Figure 1. Then the optimized Asp molecule was set as the reactant to initiate the pyrolysis reaction through direction bond breakage route and hydrogen atom transport route to seek the most possible pathway for the finally generation of NH_3 and HCN.

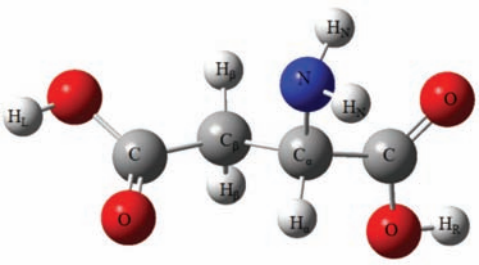

Figure 1 Stable configuration of Asp

3 Results and discussion

3.1 Reaction network of gas pyrolysis

First of all, we initiated our investigation by finding the key reaction steps during gas pyrolysis to gather a broad view of the reaction process. To map out the fit reaction network, we took a recursive "trial-and-error" approach in reference to the work of Liu[31]. First the initial bond cleavage of Asp was explored by breaking its CH, OH, NH, CN and CC bonds individually and took into the transfer of hydrogen atom (including H_α, H_β and H_N) then walked through each "likely" channel stepwise until NH_3 and HCN species were reached. The following will detail the calculated reaction networks for Asp pyrolysis through direct bond breakage and hydrogen transport processes.

3.1.1 Bond breakage and dehydrogenation

The calculated Asp pyrolysis reaction network through bond breakage is schematically summarized in Figure 2, where it aimed at achieving the most possible reaction path for the generation of NH_3 and HCN. As a starting point, we identified nine different bond-breaking and two de-H_2 pathways. The two direct H_2 generation routes are most unlikely, with extremely high reaction barriers (471.22 kJ/mol and 481.98 kJ/mol), and the next most unfavorable pathways are dehydrogenation from the acid group [-COOH] and from the [-NH_2] group due to the high electronegativity of the O atom and N atom. While the high barriers of these pathways may be expected, it is quite unanticipated to observe that the H_β-dehydrogenation is, in fact, less favorable than H_α-dehydrogenation and the direct C_α-C_β decomposition. C_α acts as the active site in the Asp molecule. And the direct C_α-C_β decomposition path is the most possible reaction process, with the lowest barrier energy (E_a) of 225.27 kJ/mole compared to other bond breakage reactions. Following the direct C_α-C_β decomposition reaction, the second most possible reaction relates to the de-H_2 from the [-NH_2] group of the generated [$CHNH_2COOH$] species, showing an E_a of 240.62 kJ/mol. Based on the first two steps, we only detected the [HCN] species released as the third step, the reaction step showed an E_a of 101.79 kJ/mol. Results imply that if the first and the second steps happen, [HCN] will

generate easily. However, the electronic properties of the reactants contribute to each reaction. In the following section, it is significant to go further into the nature of the key reaction paths.

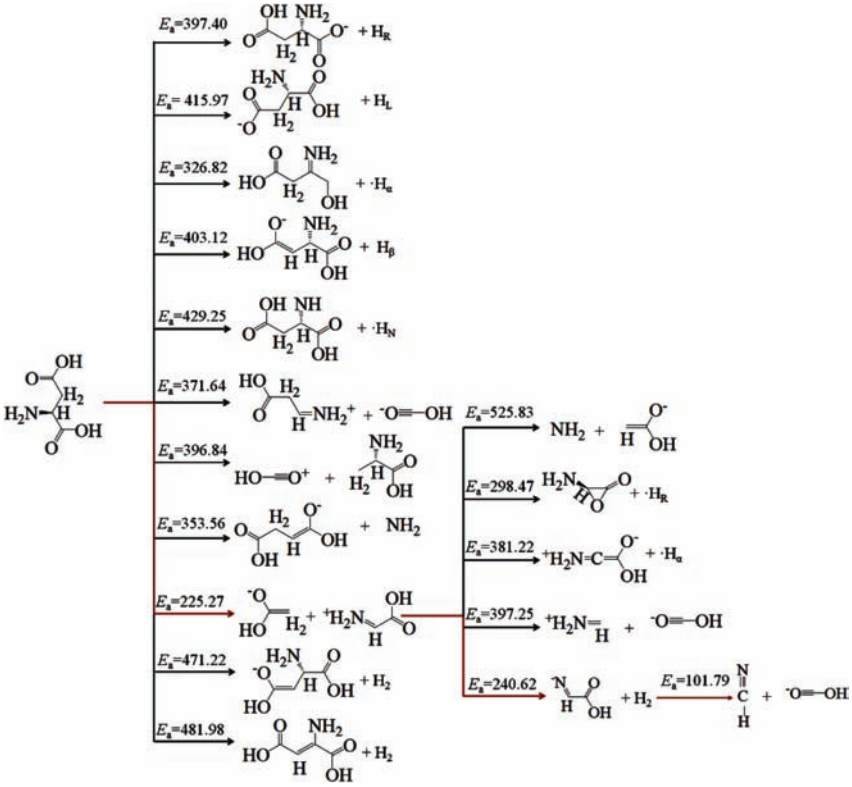

Figure 2 Reaction network initiated from the decomposition of the pure Asp molecule to the final decomposition into NH_3 and /or HCN (The reaction barriers (kJ/mol) are the barriers after the zero-point-energy correction)

3.1.2 Hydrogen transport for further decomposition of Asp

In fact, atom transport is unavoidable within the molecule during pyrolysis processes. Figure 3 schematically summarized the reaction network initiated from three different hydrogen transports (named as the *H_N-path, the H_β-path and the H_α-path*) to the final decomposition into [NH_3] and/or [HCN].

Through the *H_α-path*, H_α transport to C_β resulting in the breakage of C_α-C_β is more likely, with the lowest reaction barrier of 246.19 kJ/mol, and the next favorable pathway is H_α transport to C_N forming [-NH_3] group. Then the [-NH_3] group can decompose from the $COOHCH_2C(CH_3)COOH$ molecule and change into [NH_3] species. In additions, breakage of C_α-C_β led to the generation of [$COOHCH_3$] and $C(NH_2)COOH$ species. Because this work focused on the generation of NH_3 and HCN, we went further into the decomposition of $C(NH_2)COOH$, involving H_N transport, bond breakage and dehydrogenation. The H_N transport path is terminated by the generation of [CH(NH)COOH] species, which is related to the transport of H_N from the N atom to C_α. But the dehydrogenation of H_N forming the [C(NH)COOH] species went through a further H_N transport from N atom to C_α forming the [HCNCOOH] species, which then decomposed into [HCN] and [COOH] with the E_a of 101.79 kJ/mol.

Through the *H_N-path*, H_N transfer to the C atom of the right COOH group is more energetically accessible than the transfer to other atoms of Asp. Another H_N further transferred toward the generated $-C(OH)_2$ group, resulting in the generation of H_2O molecule. Further reactions showed far higher barrier energies than the paths for generation of [NH_3] and [HCN] following the *H_α-path* in Figure 3. Therefore, it needs not to discuss further reactions following the *H_N-path*.

For the *H_β-path*, all the reactions are more energetically close while compared to the *H_N-path* and the *H_α-path*, since H_α and H_N are more active than H_β. For H_α and H_N, especially for H_α, more density of states are observed at energies close to the Fermi level, while they are much lower for H_N. Obviously, the total

density of state for H_α with its high electronic states allows for an energetically easier excitation and renders H_α thereby more reactive than the H_N and H_β.

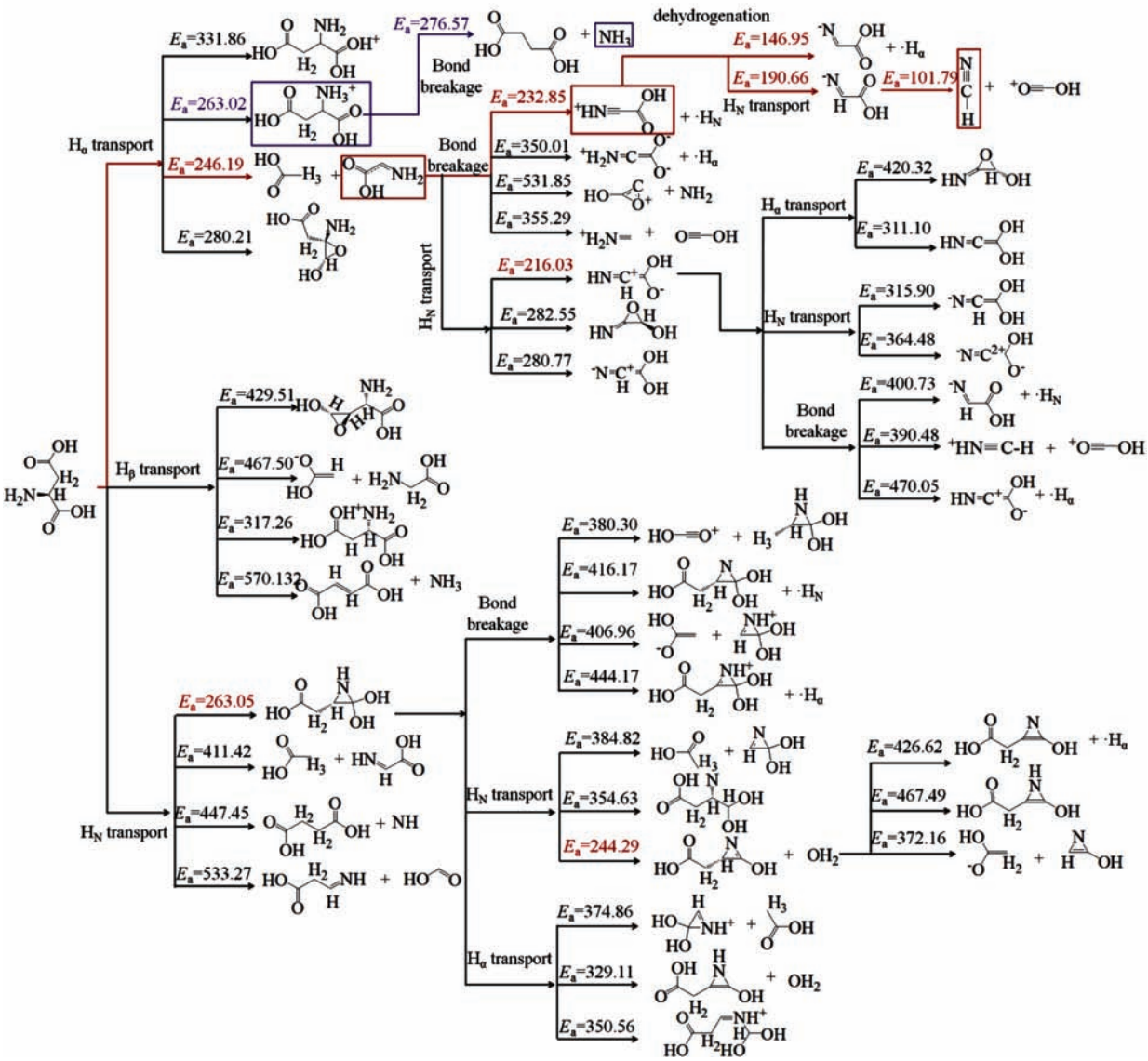

Figure 3 Reaction network initiated from hydrogen transport of the pure Asp molecule to the final decomposition into NH_3 and /or HCN (The reaction barriers (kJ/mol) are the barriers after the zero-point-energy correction)

3.2 HCN emission from Asp pyrolysis

Depending on Figures 2 and 3, this study focused on the possible reaction path with the lowest reaction barrier for the generation of HCN, where two key reaction paths can be observed. Figure 4a shows the calculated potential energy profiles for the key reaction path for Asp decomposition into HCN. The reactions initiate from the optimized geometries of the pure Asp molecule. Then the negative atomic charge population of C_α and C_β lead to the decomposition of C_α-C_β more accessible than other decomposition channels as showed in Figure 2. The activation energy (E_a) and reaction energy (E_r) for this step are 225.27 kJ/mol and 212.62 kJ/mol, respectively, which is an endothermic process. The atomic charge distribution of the system at the critical points, i.e. initial state, transition state and final state, of the reaction shows mainly partial electron transfer from C_α to C_β. With atomic charge repopulation, $[COOHCH_2CH(NH_2)COOH]$ decomposition into $[COOHCH_2]$ and $[CH(NH_2)COOH]$ through one-step reaction mechanism.

Since N element is un-appear in $[COOHCH_2]$, the step-2 in Figure 4a initiates from the optimized geometries of $[CH(NH_2)COOH]$ which crosses the barrier of 225.27 kJ/mol and changes into a free hydrogen molecule and the [HCNCOOH] species with the E_r of

200.60 kJ/mol. Then, if gaining an activation energy of 101.79 kJ/mol, [HCNCOOH] would decompose into the [HCN] and [COOH] species.

The above steps follow one-step reaction mechanism, and the chain reaction process can be concluded as follows:

$[COOHCH_2CH(NH_2)COOH] \rightarrow [COOHCH_2] + [CH(NH_2)COOH]$ (Step-1 in Figure 4a)

$[CH(NH_2)COOH] \rightarrow [HCNCOOH] + [H_2]$ (Step-2 in Figure 4a)

$[HCNCOOH] \rightarrow [HCN] + [COOH]$ (Step-3 in Figure 4a)

Step-2 is the speed control step from the generation of [HCN]. The highest barrier energy for [HCN] generation is 240.62 kJ/mol. And the reaction energy for the whole process for generation of $[NH_3]$ is 505.77 kJ/mol.

Then, taking the hydrogen transport to the neighbor sites within the molecule into consideration, it was found that another key route can also lead to the generation of HCN. Figure 4b illustractes the calculated potential energy profiles for the key reaction path for Asp decomposition into HCN, which initiated from H_α transport from C_α to the C_β within the Asp molecule.

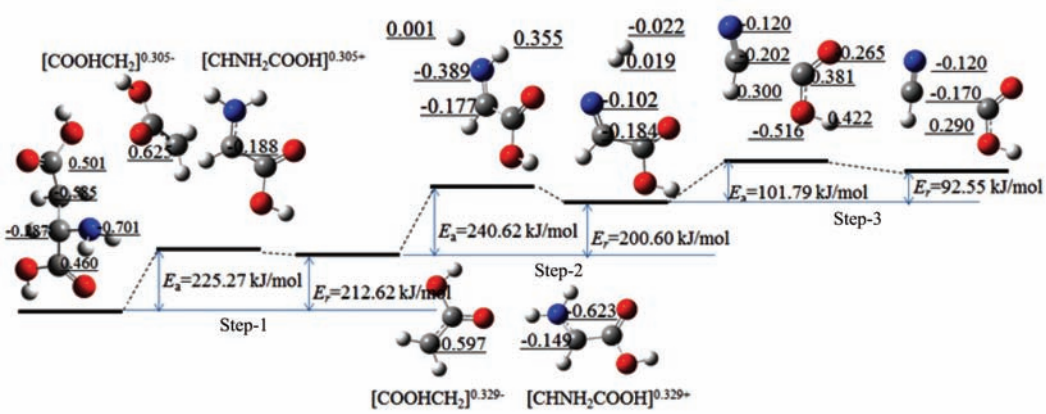

a.

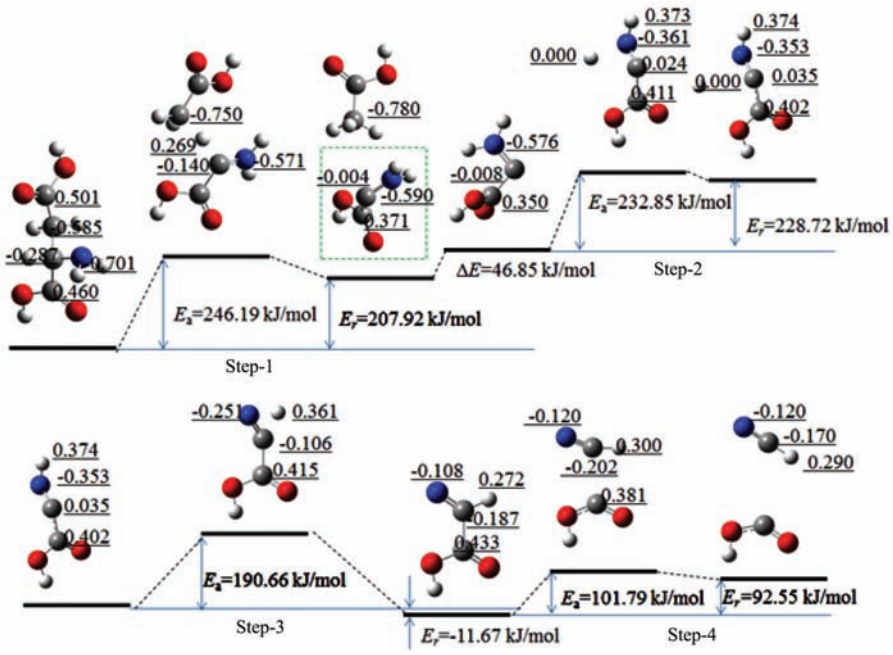

b.

Figure 4 Calculated potential energy profiles for the key reaction path for Asp decomposition into HCN, (a) without and (b) with the considering of hydrogen transport (Charges of the atoms are underlined)

While Asp crossed the energy barrier of 246.19 kJ/mol, H_α-C_α bond broke and moved toward C_β at the bridge site between C_α and C_β, resulting in the breakage of the C_α and C_β bond, showing that the H_α-C_α bond length and H_α-C_β bond length are 1.273 Å and 1.441 Å, respectively. During this process, electron loss at C_α and enriched at C_β, indicating charge transported from C_α to C_β. Then H_α further moved and bound to C_β,

as well as charge further repopulation, the Asp molecule broke into [$COOHCH_3$] and [$H_2NCCOOH$] species, giving the E_r of 207.92 kJ/mol. This process is endothermic. [$H_2NCCOOH$] species jumped into another stable molecular state if obtaining an energy of 46.85 kJ/mol during the pyrolysis process. Further activated by the relatively high temperature, the [$H_2NCCOOH$] species crossed an energy barrier of 232.85 kJ/mol, leading to the generation of an atomic hydrogen and a neutral molecule [HNCCOOH]. However, the H_N prefers to transport to C_α rather than other processes within the [HNCCOOH] molecule (as showed in Figure 4). The reaction of [HNCCOOH] changing into [NCHCOOH] shows the E_a and E_r of 190.66 kJ/mol and −11.67 kJ/mol. This process is exothermic. Then [HNCHCOOH] decomposes into the [HCN] and [COOH] species, the same process as Step-3 in Figure 4a.

All the steps processes in Figure 4b can be concluded as follows:

[$COOHCH_2CH(NH_2)COOH$] → [$COOHCH_3$] + [$H_2NCCOOH$] (Step-1 in Figure 4b)

[$H_2NCCOOH$] → [NCHCOOH] + [H] (Step-2 in Figure 4b)

[HNCCOOH] → [NCHCOOH] (Step-3 in Figure 4b)

[CNCHOOH] → [HCN] + [COOH] (Step-4 in Figure 4b)

H_α transport from C_α to C_β and the resulted C_α-C_β bond breakage act as the speed control step from the generation of [HCN], corresponding to Step-1 in Figure 4b. The highest barrier energy for [HCN] generation following this mechanism is 246.19 kJ/mol. And the reaction energy for the whole process for the generation of [HCN] is 564.37 kJ/mol. Both the E_a and the E_r for the generation of [HCN] in Figure 4b are slightly higher than those in Figure 4a, suggesting that the direct decomposition of Asp molecule initiating from C_α-C_β bond breakage is more accessible than initiating from H_α transport route.

It was further verified that generated [HCN] species is HCN by comparing its density of state (DOS) to that of the pure HCN molecule. Figure 5 plot the DOS for both [HCN] and the pure HCN molecule. From Figure 5, it could be observed no changes in the DOS for the case of [HCN] and the pure HCN molecule. Around the Fermi level (E_f = 0.0 eV), between −7 eV and −6 eV, and between −15 eV and −14 eV, DOS of the [HCN] shows three sharp peaks which corresponds to π bond between C atom and N atom ($\pi_{C\text{-}N}$), σ bond between C atom and N atom ($\sigma_{C\text{-}N}$), σ bond between C atom and H atom ($\sigma_{C\text{-}H}$), respectively. The $\pi_{C\text{-}N}$ contributes the highest occupied molecular orbital (HOMO), while the d bond between C atom and N atom ($d_{C\text{-}N}$) around 5 eV contributes to the lowest unoccupied molecular orbital (LUMO), corresponding to the work of Ali Shokuhi Rad[32]. However, though the DOS of the generated [HCN] left shifts, the characteristic peaks of the DOS corresponds to $d_{C\text{-}N}$, $\pi_{C\text{-}N}$, $\sigma_{C\text{-}N}$ and $\sigma_{C\text{-}H}$, respectively. It was calculated that N-H bond length and H–N–H bond angle for NH_3 are 1.162 Å and 1.077 Å, respectively, which are in agreement with those of 1.160 Å, 1.075 Å for the generated HCN on Pt[33], respectively. Results verified the generated [HCN] as HCN molecule.

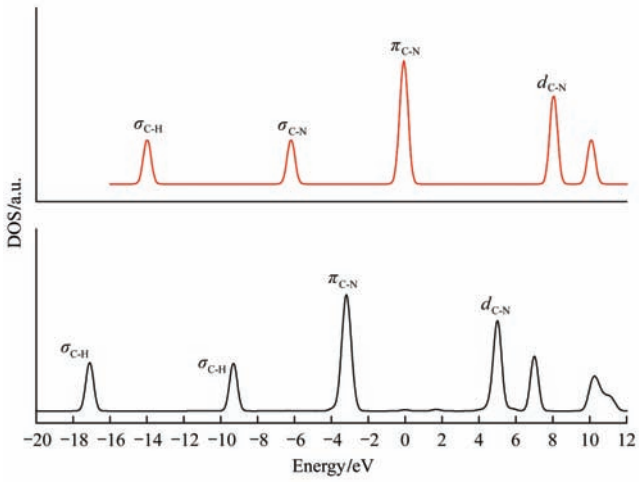

Figure 5 Total electronic densities of states for [HCN] and the pure HCN molecule

3.3 NH_3 emission from Asp pyrolysis

Figure 6 shows the same energy profiles as Figure 5 but for the key reaction leading to the generation of the [NH_3] species. The reaction initiated from the stable Asp molecule. The H_α atom moves toward the N atom, bonding to the bridge site of the N and O atom within the Asp molecule. Then H_α approached further to the N atom, the H atom lost more electron density than that at the initiate state, due to the higher electronegativity of N atom than that of C_α, which led to the formation of [NH_3] group. This process requires barrier energy of 263.02 kJ/mol. And the reaction energy is 104.42 kJ/mol.

Further the product crosses the barrier of 276.57 kJ/mol and obvious charge repopulation occurs, resulting in de-NH_3. The reaction energy for the whole process for generation of [NH_3] is 326.46 kJ/mol.

The generation of [NH_3] follows a two-step chain reaction mechanism:

[$COOHCH_2CH(NH_2)COOH$]→[$COOHCH_2C(NH_3)COOH$] (Step-1 in Figure 6)

[$COOHCH_2C(NH_3)COOH$]→[$COOHCH_2CCOOH$]+[NH_3] (Step-2 in Figure 6)

where, the Step-1 is the rate-determining step.

The highest barrier energy for [NH_3] generation following this mechanism is 276.57 kJ/mol, which is higher than those for the generation of HCN through the two key pathways discussed above. And the reaction energy for the whole process for generation of [NH_3] is 36246 kJ/mol.

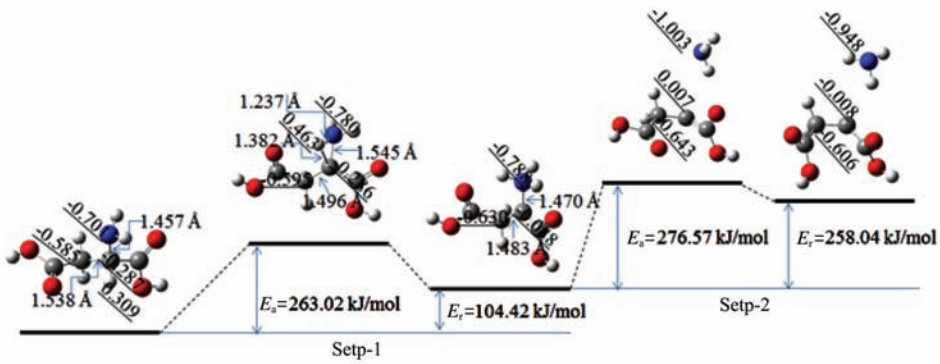

Figure 6 Calculated potential energy profiles for the key reaction path for Asp decomposition into HCN, with the considering of hydrogen transport (Charges of the atoms are underlined; distances are given in units of Å)

To validate the theoretical prediction of the generated NH_3 molecule, the DOS of [NH_3] species has been carried out in comparison with that of a pure NH_3 molecule, which is shown in Figure 7.

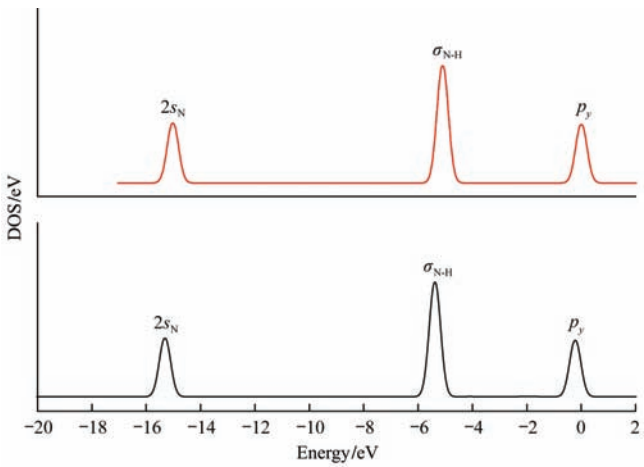

Figure 7 Total electronic densities of states for [NH_3] and the pure NH_3 molecule

Figure 7 observes that the DOS of [NH_3] is almost the same as that of the pure NH_3 molecule, showing three characteristic peaks around and below the E_f, which are for 2s of N atom ($2s_N$), σ bond between H atom and N atom (σ_{N-H}), the $2p_y$ electrons of N atom of the [NH_3] species and the pure NH_3 molecule, respectively. Calculated N-H bond length and H–N–H bond angle for NH_3 were 1.028 Å and 105.973°, respectively, which are in agreement with the reported experimental values of 1.02 Å and 106.7°, respectively[34,35]. Results verified the generated NH_3 molecule.

While comparing the barrier energy for the generation of both NH_3 and HCN through the direct C_α-C_β bond breakage route and the H_α transport route, it was found that HCN generates easier than NH_3 during the pyrolysis of Asp process, which corresponds to the previous results[34,35].

3.4 Kinetics analysis

To address the trends in NH_3 and HCN generation more accurately, kinetic models are required in order to treat the different time scales associated with the temperature during the pyrolysis of Asp. It is generally agreed that, the apparent reaction rate of the whole chain reaction for generation of NH_3 and HCN depend on the step with the highest barrier energy (generally taken as the rate-determining step).

Therefore, the reaction rate for HCN generation follows the direct Asp decomposition processes and the *H_α-path* processes depends on the following two steps, as analyzed above:

$[CH(NH_2)COOH] \rightarrow [HCNCOOH] + [H_2]$ (Step-2 in Figure 4a)

$[COOHCH_2CH(NH_2)COOH] \rightarrow [COOHCH_3] + [H_2NCCOOH]$ (Step-1 in Figure 4b)

And the reaction rate for NH_3 generation following H_α-*path* processes depends on the following step, as analyzed above:

$[COOHCH_2C(NH_3)COOH] \rightarrow [COOHCH_2CCOOH] + [NH_3]$ (Step-2 in Figure 6)

We applied a simple phenomenological model to carry out the trends. The net reaction rates for generation of HCN and NH_3 are written as:

$$R_{HCN}(\text{Step}-2 \text{ in Figure 4a}) = \vec{k}c_{[CH(NH_2)COOH]} - \overleftarrow{k}c_{[HCNCOOH]} \times c_{[H_2]}$$

$$R_{HCN}(\text{Step}-1 \text{ in Figure 4b}) = \vec{k}c_{[COOHCH_2CH(NH_2)COOH]} - \overleftarrow{k}c_{[COOHCH_3]} \times c_{[H_2NCCOOH]}$$

$$R_{NN_3}(\text{Step}-2 \text{ in Figure 6}) = \vec{k}c_{[COOHCH_2CH(NH_2)COOH]} - \overleftarrow{k}c_{[COOHCH_2CCOOH]} \times c_{[NH_3]}$$

where, $\vec{k}$ and $\overleftarrow{k}$ are forward rate constant and backward rate constant, respectively; C is the concentration term for the corresponding reaction component.

The rate constants could be written as:

$$k_i = \frac{k_B T}{h} \frac{f^{\neq}}{\prod_j f_j} \exp(\frac{-E_i}{RT})$$

where, E_i is the activation free energy of step i. The degree of freedom for the reaction component j in each reaction step is given by:

$$f_j = f_t \cdot f_r \cdot f_v$$

where, f_t, f_r and f_v is the translational, rotational, and vibrational degree of freedom, respectively.

Since gasification temperature for Asp must be higher than its melt point (>573K), Figure 8 depicts the reaction rates:

$R_{HCN}[R_{HCN} = R_{HCN}(\text{Step}-2 \text{ in Figure 4a}) + R_{HCN}(\text{Step}-1 \text{ in Figure 4b})]$,

and $R_{NH_3}[R_{NH_3} = R_{NH_3}$ (Step − 2 in Figure 6), correlated condition are under 673 K, 773 K, 873 K, 973 K and 1073 K, with the concentration of the reactant around 100 mol/L, according to its vapor density 5 (*vs* air) and neglecting the concentration term of the products respectively. It can be seen from Figure 8, HCN should be released before NH_3 during pyrolysis of Asp, and more HCN can be tested in comparison with NH_3, corresponding to the experimental results[36]. The relation between reaction rate and temperature provides the fundamental understanding of reasonable operation for Asp pyrolysis.

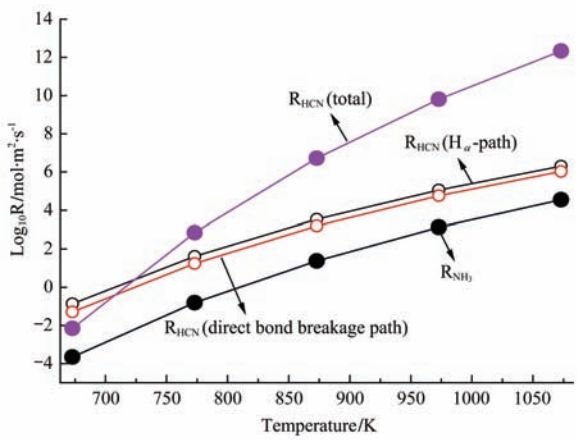

Figure 8 Reaction rate for NH_3 and HCN generation from Asp pyrolysis under different temperature

4 Conclusions

In this research, the reaction networks of Asp pyrolytic reactions initiate from direct bond breakage and hydrogen transfer within the molecule were studied through DFT calculations. Two key reaction pathways were proposed for the generation of HCN, where one follows the direct bond breakage initiating from C_α-C_β through a three-step reaction processes, $[COOHCH_2CH(NH_2)COOH] \rightarrow [COOHCH_2] + [CH(NH_2)COOH]$, $[CH(NH_2)COOH] \rightarrow [HCNCOOH] + [H_2]$, and $[HCNCOOH] \rightarrow [HCN] + [COOH]$, the highest barrier energy for [HCN] generation is 240.62 kJ/mol. And the reaction energy for the whole process for generation of $[NH_3]$ is 505.77 kJ/mol; and the other follows the transfer of H_α from C_α to C_β resulting a four step mechanism, $[COOHCH_2CH(NH_2)COOH] \rightarrow [COOHCH_3] + [H_2NCCOOH]$, $[HNCCOOH] \rightarrow [HNCCOOH] + [H]$, $[HNCCOOH] \rightarrow [NCHCOOH]$, and $[HCNCOOH] \rightarrow [HCN] + [COOH]$, the highest barrier energy for [HCN] generation following these mechanism is 246.19 kJ/mol. While the transfer of H_α from C_α to N atom of Asp, a two-step mechanism contributes to the generation of NH_3, $[COOHCH_2CH(NH_2)COOH] \rightarrow [COOHCH_2C(NH_3)COOH]$ and

$[COOHCH_2C(NH_3)COOH] \rightarrow [COOHCH_2CCOOH] + [NH_3]$, the highest barrier energy for $[NH_3]$ generation following these mechanism is 276.57 kJ/mol and the reaction energy for the whole process for generation of $[NH_3]$ is 36246 kJ/mol. Results demonstrate that HCN generates easier than NH_3 during the pyrolysis of Asp. Moreover, kinetic reaction models for the generation of HCN and NH_3 under various temperatures based on speed control method in each key reaction pathway were obtained. Tuning the properties of the active site C_α and the key reaction routes will favor the efficient and selective catalytic pyrolysis of Asp and other kinds of amino acids to control the emission of NO_x and N_2O precursors (NH_3 and HCN).

Acknowledgments

The authors wish to thank the National Natural Science Foundation of China (51106051, 51206044), the National Science Foundation of China (71273090, 71573084), the Fundamental Research Funds for the Central Universities (2016YQ07, 2015QN09, 2014MS36, 2014ZD14), the Beijing Natural Science Foundation (3132017) and "111" Project (B12034).

[References]

[1] Trinnaman J, Clarke A. World energy council: survey of energy resources for biomass. London, UK: Elsevier, 2004.

[2] Tian F J, Wu H W, Yu J L, Lachlan J M, Konstantinidis S, Hayashi J, et al. Formation of NO_x precursors during the pyrolysis of coal and biomass. Part VIII. Effects of pressure on the formation of NH_3 and HCN during the pyrolysis and gasification of Victorian brown coal in steam. Fuel, 2005; 84(16): 2102–2108.

[3] Tian F J, Yu J L, McKenzie L J, Hayashi J, Li C Z. Formation of NO_x precursors during the pyrolysis of coal and biomass. Part IX. Effects of coal ash and externally loaded-Na on fuel-N conversion during the reforming of coal and biomass in steam. Fuel, 2006; 85(10-11): 1411–1417.

[4] Tian F J, Yu J L, McKenzie L J, Hayashi J, Li C Z. Conversion of fuel-N into HCN and NH_3 during the pyrolysis and gasification in steam: a comparative study of coal and biomass. Energ. Fuel, 2007; 21(2): 517–521.

[5] Giuntoli J, de Jong W, Verkooijen A H M, Piotrowska P, Zevenhoven M, Hupa M. Combustion characteristics of biomass residues and biowastes: fate of fuel nitrogen. Energ. Fuel, 2010; 24(10): 5309–5319.

[6] Tian Y, Zhang J, Zuo W, Chen L, Cui Y N, Tan T. Nitrogen conversion in relation to NH_3 and HCN during microwave pyrolysis of sewage sludge. Environ. Sci. Technol., 2013; 47(7): 3498–3505.

[7] Stubenberger G, Scharler R, Zahirović S, Obernberger I. Experimental investigation of nitrogen species release from different solid biomass fuels as a basis for release models. Fuel, 2008; 87(6): 793–806.

[8] Tian F J, Yu J L, Mckenzie L J, Hayashi J, Li C Z. Conversion of fuel-N into HCN and NH_3 during the pyrolysis and gasification in steam: a comparative study of coal and biomass. Energ. Fuel., 2007; 21(2): 517–521.

[9] Darvell L I, Brindley C, Baxter X C, Jones J M, Williams A. Nitrogen in biomass char and its fate during combustion: a model compound approach. Energ. Fuel, 2012; 26(11): 6482–6491.

[10] Yuan S, Zhou Z J, Li J, Wang F C. Nitrogen conversion during rapid pyrolysis of coal and petroleum coke in a high-frequency furnace. Appl. Energ., 2012; 92: 854–859.

[11] Yuan S, Chen X L, Li W F, Liu H F, Wang F C. Nitrogen conversion under rapid pyrolysis of two types of aquatic biomass and corresponding blends with coal. Bioresource Technol., 2011, 102(21): 10124–10130.

[12] Scicchitano P, Carbonara S, Ricci G, Mandurino C, Locorotondo M, Bulzis G, et al. HCN channels and heart rate. Molecules, 2012; 17(4): 4225–4235.

[13] Ren Q Q, Zhao C S. Evolution of fuel-N in gas phase during biomass pyrolysis. Renew. Sust. Energ. Rev., 2015; 50: 408–418.

[14] Becidan M, Skreiberg Ø, Hustad J E. NO_x and N_2O precursors (NH_3 and HCN) in pyrolysis of biomass residues. Energ. Fuel, 2007; 21(2): 1173–1180.

[15] Hansson K M, Samuelsson J, Åmand L E, Tullin C. The temperature's influence on the selectivity between HNCO and HCN from pyrolysis of 2, 5-diketopiperazine and 2-Pyridone. Fuel, 2003; 82(18): 2163–2172.

[16] Hansson K M, Samuelsson J, Tullin C, Åmand L E. Formation of HNCO, HCN, and NH_3 from the pyrolysis of bark and nitrogen-containing model compounds. Combust. Flame, 2004; 137(3): 265–277.

[17] Yuan S, Zhou Z J, Li J, Chen X L, Wang F C. HCN and NH_3 released from biomass and soybean cake under rapid pyrolysis. Energ. Fuel, 2010; 24(11): 6166– 6171.

[18] Ren Q Q, Zhao C S. NO_x and N_2O precursors from biomass pyrolysis: role of cellulose, hemicellulose and lignin. Environ. Sci. Technol., 2013; 47(15): 8955– 8961.

[19] Ren Q Q, Zhao C S, Wu X, Liang C, Chen X P, Shen J Z, et al. Effect of mineral matter on the formation of NO_x precursors during biomass pyrolysis. J. Anal. Appl. Pyrol., 2009; 85(1-2): 447–453.

[20] Ren Q Q, Zhao C S. NO_x and N_2O precursors from biomass pyrolysis: nitrogen transformation from amino acid. Environ. Sci. Technol., 2012; 46(7): 4236–4240.

[21] Ren Q Q, Zhao C S. NOx and N_2O precursors (NH_3 and HCN) from biomass pyrolysis: interaction between amino acid and mineral matter. Appl. Energ., 2013; 112(4): 170–174.

[22] Perdew J P, Burke K, Wang Y. Generalized gradient approximation for the exchange-correlation hole of a many-electron system. Phys. Rev. B., 1996; 54(23): 16533–16537.

[23] Perdew J P, Burke K, Ernzerhof M. Generalized gradient approximation made simple. Phys. Rev. Lett., 1996; 77(18): 3865–3868.

[24] Delley B. An all-electron numerical method for solving the local density functional for polyatomic. molecules. J. Chem. Phys., 1990; 92(1): 508–517.

[25] Delley B. From molecules to solids with the $DMol^3$ approach. J. Chem. Phys., 2000; 113(18): 7756–7764.

[26] Delley B. Fast calculation of electrostatics in crystals and large molecules. J. Phys. Chem., 1996; 100(15): 6107–6110.

[27] Kudin K N, Ozbas B, Schniepp H C, Prud'Homme R K, Aksay I A, Car R. Raman spectra of graphite oxide and functionalized graphene sheets. Nano. Lett., 2008; 8(1): 36–41.

[28] Govind N, Petersen M, Fitzgerald G, King-Smith D, Andzelm J. A generalized synchronous transit method for transition state location. Comput. Mater. Sci., 2003; 28(2): 250–258.

[29] Qin W, Wu L N, Zheng Z M, Dong C Q, Yang Y P. Lignin hydrolysis and phosphorylation mechanism during phosphoric acid-acetone pretreatment: a DFT study. Molecules, 2014; 19(12): 21335–21349.

[30] Zhang Y Y, Liu C, Chen X. Unveiling the initial pyrolytic mechanisms of cellulose by DFT study. J. Analyt. Appl. Pyrol., 2015; 113: 621–629.

[31] Wang H F, Liu Z P. Comprehensive mechanism and structure-sensitivity of ethanol oxidation on platinum: New transition-state searching method for resolving the complex reaction network. J. Am. Chem. Soc., 2008; 130(33): 10996–11004.

[32] Rad A S, Zardoost M R, Abedini E. First-principles study of terpyrrole as a potential hydrogen cyanide sensor: DFT calculations. J. Mol. Model, 2015; 21: 273.

[33] Deng Z G, Lu X Q, Wen Z Q, Wei S X, Zhu Q, Jin D L, et al. Decomposition mechanism of methylamine to hydrogen cyanide on Pt(III): selectivity of the C-H, N-H and C-N bond scissions. RSC. Adv., 2014; 24(4): 12266– 12274.

[34] Lide D R. CRC Handbook of Chemistry and Physics (67th ed). Boca Raton, FL: CRC, 1983.

[35] Lide D R. CRC Handbook of Chemistry and Physics. New York: Wiley, 1996.

[36] Ren Q Q. Nitrogen transfer mechanism during thermal utilization of agricultural straw. Nanjing: Southeast University, 2011.